




Plasmons in three-dimensional superconductors

T. Repplinger ¹, S. Klimin ², M. Gélédan ¹, J. Tempere,² and H. Kurkjian ¹

¹*Laboratoire de Physique Théorique, Université de Toulouse, CNRS, UPS, 31400 Toulouse, France*

²*TQC, Universiteit Antwerpen, Universiteitsplein 1, B-2610 Antwerp, Belgium*



(Received 27 January 2022; revised 24 November 2022; accepted 28 November 2022; published 10 January 2023)

We study the plasma branch of an homogeneous three-dimensional electron gas in an s -wave superconducting state. Although a sum rule guarantees that the departure of the plasma branch always coincides with the plasma frequency ω_p , the dispersion and lifetime of plasmons is strongly affected by the presence of the pair condensate, especially when ω_p is close to the pair-breaking threshold 2Δ . When ω_p is between 1.7Δ and 2Δ , the level repulsion is strong enough to give the plasma branch an anomalous, downward dispersion and a dispersion minimum strictly lower than ω_p . Then for $\omega_p > 2\Delta$, plasmons damp out in pair-breaking excitations, acquiring a small damping rate at zero temperature, which we compute in a non-perturbative way. Finally, the density-density response function displays a resonance near 2Δ (not to be confused with the amplitude mode), which can beat with the main plasma resonance, and subsists for ω_p large compared to Δ , thereby distinguishing charged from neutral condensates.

DOI: [10.1103/PhysRevB.107.014504](https://doi.org/10.1103/PhysRevB.107.014504)

I. INTRODUCTION

Despite being a very mature experimental platform, supporting numerous technical applications, superconductors still hold some of the most fundamental open questions of many-body physics. The impressively high critical temperature (T_c) and the unconventional Cooper pairing in cuprates and iron-based superconductors are the most famous of those fascinating questions. However, even some properties of conventional Bardeen-Cooper-Schrieffer (BCS) superconductors are still intensively discussed, such as the existence of an amplitude collective mode [1–3], reminiscent of the Higgs mode in high-energy physics.

In fact, even for such usual behavior as plasma oscillations (the collective modes of the electronic density), superconductors are still not fully understood. In a pioneering work, Anderson [4] has shown that the phononic (Goldstone) branch that exists in a neutral fermionic condensate acquires a gap corresponding to the plasma frequency ω_p in presence of long-range Coulomb interaction. This mechanism later became famous due to its analogy with the phenomenon of mass acquisition in high-energy physics. The work of Anderson has then been revisited in the context of high- T_c superconductivity [5–9], and nuclear/neutronic matter [10]. While Anderson focused on the regime of large ω_p , the frequency of transverse plasmons in layered materials (such as cuprates) softens to an acoustic dispersion, such that in the superconducting phase an undamped plasma branch can be expected [11–14] below the pair-breaking threshold 2Δ . While a sum-rule [9] guarantees that the branch always departs from ω_p , the dispersion relation was shown [15–17] to approach the phononic law ($\omega_{q,n}$) of neutral fermionic condensates as $\sqrt{\omega_p^2 + \omega_{q,n}^2}$ in the limit $\omega_p \ll 2\Delta$.

In both limits of large and small ω_p , the dispersion of plasmons is thus similar to the dispersion in the normal phase, and

no significant effect of superconductivity has been reported so far. On the contrary, our study identifies a significant distortion of the plasma resonance caused by superconducting electrons. The distortion is largest when ω_p is close to 2Δ , but even for large ω_p the pair-breaking continuum bears the trace of Coulomb interactions.

We consider the reference situation of an isotropic three-dimensional (3D) s -wave superconductor but our study can be readily extended to layered geometries or anisotropic pairing. We identify three main differences between normal and superconducting plasmons. First, when $1.696\Delta < \omega_p < 2\Delta$, the plasma branch is repelled by the pair-breaking threshold, and acquires an anomalous dispersion, with a negative curvature and thus a minimum strictly below ω_p . Second, at $\omega_p > 2\Delta$, plasmons are damped (even at zero temperature) and decay by breaking Cooper pairs. Last, but not least, we find a second resonance in the low-energy region of the pair-breaking continuum, separated from the main plasma peak. This second peak is particularly intense when ω_p is near 2Δ and leads to spectacular beatings in the time evolution of a perturbation of the electronic density. The peak, however, subsists in the regime $\omega_p \gg \Delta$, and is thus a fingerprint of fermionic condensates with long-range interactions.

By assessing the influence of superconductivity on density oscillations, our study can guide practical use of plasmonics to probe and manipulate superconducting materials [14,18,19]. The low-energy plasmons we describe may also affect the critical temperature through their zero-point motion [20].

II. DISPERSION EQUATION

We study a homogeneous electron gas evolving in a cubic volume V with an average density ρ , defining the Fermi wavenumber $\rho = k_F^3/3\pi^2$. Electrons interact through both the long-range Coulomb potential $V_C(r) \propto 1/r$ and a short-range

part, responsible for s -wave Cooper pairing, and modelled by a contact potential of coupling constant g :

$$V(\mathbf{r}_1, \mathbf{r}_2) = g\delta(\mathbf{r}_1 - \mathbf{r}_2) + V_C(\mathbf{r}_1 - \mathbf{r}_2). \quad (1)$$

In terms of the electron mass m and wavenumber q , the Fourier transform of the Coulomb potential is $V_C(q) = m\omega_p^2/\rho q^2$ (we use $\hbar = k_B = 1$ throughout the article).

We imagine that the system is driven at fixed frequency ω and wavenumber q by an external field (for example, an electromagnetic field) and we study the collective response within linear response theory. In more standard situations this response can be described by London electrodynamics [21] (a long wavelength effective theory), but for the present purpose of describing the interplay between plasma waves and Cooper pairing, a microscopic theory, such as the Random Phase Approximation (RPA) is unavoidable. Such an approach results in a linear system [22] relating the density $\delta\rho$ and pair-field fluctuations (in phase $\delta\theta$ and modulus $\delta|\Delta|$) to the corresponding drive fields u_θ , $u_{|\Delta|}$, and u_ρ :

$$\begin{pmatrix} 2i\Delta\delta\theta(\mathbf{q}, \omega) \\ 2\delta|\Delta(\mathbf{q}, \omega)| \\ 2V_C(q)\delta\rho(\mathbf{q}, \omega) \end{pmatrix} = \chi(\omega, \mathbf{q}) \begin{pmatrix} u_\theta(\mathbf{q}) \\ u_{|\Delta|}(\mathbf{q}) \\ u_\rho(\mathbf{q}) \end{pmatrix}. \quad (2)$$

The 3×3 response matrix χ , which incarnates the coupling between density and pairing fluctuations in superconductors, is expressed in terms of the bare propagator Π as $\chi = (D - \Pi)^{-1}\Pi$ with

$$D \equiv \begin{pmatrix} V/g & 0 & 0 \\ 0 & V/g & 0 \\ 0 & 0 & V/2V_C(\mathbf{q}) \end{pmatrix}. \quad (3)$$

The spectrum of the collective modes corresponds to the poles of χ , hence to the zeros of $M = D - \Pi$:

$$\det M_\downarrow(z_{\mathbf{q}}, \mathbf{q}) = 0. \quad (4)$$

When damping mechanisms are active (for example, at $\omega > 2\Delta$ or at nonzero temperature), a branch cut appears on the real axis, representing the coupling to the continuum of decay channels. In such situation, we use recently develop techniques [23–25] to extract the pole in an analytic continuation through the branch cut (in Eq. (4), M_\downarrow denotes such an analytic continuation of M). This study focuses on the typical weak-coupling regime of superconductors, with Δ much smaller than the Fermi energy ϵ_F , and the excitation wavelength comparable to the Cooper pair size $\xi = k_F/2m\Delta$. In this regime, the fluctuation of the modulus of the order parameter are decoupled from the phase-density fluctuations:

$$\det M_\downarrow = 0 \iff M_{11,\downarrow}M_{33,\downarrow} - M_{13,\downarrow}^2 = 0 \text{ or } M_{22,\downarrow} = 0. \quad (5)$$

The second condition gives rise to the “pair-breaking” or “Higgs” modulus mode, which in the weak-coupling regime is insensitive to Coulomb interactions [24,26]. Here, we study the density-phase modes, fulfilling the first condition.

III. ANOMALOUS DISPERSION OF LONG WAVELENGTH PLASMONS

We first study analytically the plasmon dispersion in the limit $q \ll 1/\xi$, where, by analogy with the normal case [27],

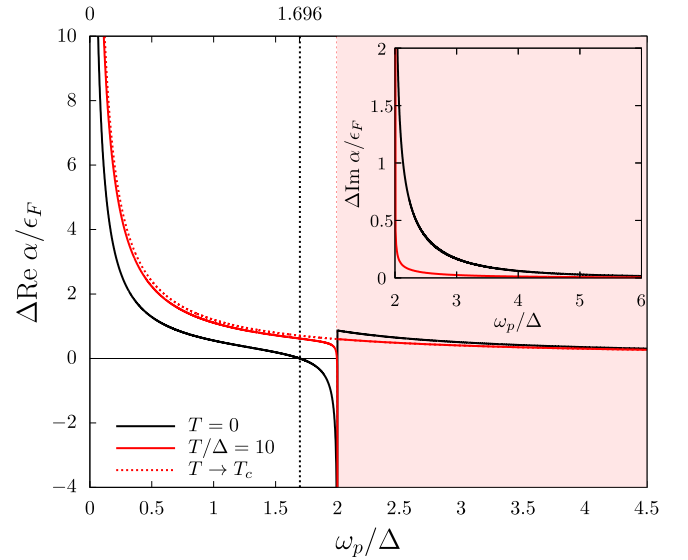


FIG. 1. Dispersion parameter $\text{Re } \alpha$ (multiplied by Δ/ϵ_F to have a finite weak-coupling limit), in function of the plasma frequency at zero (black curve) and high temperature (red curve). The normal dispersion $6\epsilon_F/5\omega_p$ is shown by the red dotted curve. The value where α changes sign at $T = 0$ is indicated by the black dotted line. Inset: the damping parameter $\text{Im } \alpha$, which becomes nonzero inside the pair-breaking continuum $[2\Delta, +\infty[$ (red area).

one can expect the quadratic law [7]:

$$z_{\mathbf{q}} = \omega_0 + \alpha \frac{q^2}{2m} + O(q^4). \quad (6)$$

A sum rule [9] (see Eq. (A8)) guarantees that the origin ω_0 of the plasma branch always coincides with the plasma frequency

$$\omega_0 = \omega_p, \quad (7)$$

as in the normal phase. Superconductivity, however, greatly influences the departure of the plasma branch through its curvature α . At zero temperature, we derive the fully analytic expression of α :

$$\alpha = \frac{6\epsilon_F}{5\omega_p} - \frac{32\epsilon_F}{15\omega_p} \frac{\Delta^2 \arcsin(\omega_p/2\Delta)}{\omega_p \sqrt{4\Delta^2 - \omega_p^2}}, \quad (8)$$

which is shown as a black curve on Fig. 1. In the conventional limit $\omega_p \gg 2\Delta$, we recover the normal plasmon dispersion [27] $\alpha \rightarrow 6\epsilon_F/5\omega_p$. Highly energetic density waves are thus insensitive to the weak pairing between electrons. In the opposite “quasiphononic” limit $\omega_p \ll 2\Delta$, which corresponds to the experimental situation of Refs. [13,16], rather than expanding for fixed z as prescribed by Eq. (6), one should expand [15] for $q \rightarrow 0$ while keeping z/v_F comparable to q . This yields¹

$$z_{\mathbf{q}} \xrightarrow[\substack{q \rightarrow 0 \\ cq/\omega_p \text{ fixed}}]{} \sqrt{\omega_p^2 + c^2 q^2}, \quad (9)$$

¹Note that this is consistent with the behavior of α in the limit $\omega_p/\Delta \rightarrow 0$.

where $c = v_F/\sqrt{3}$ is the speed-of-sound of the weakly interacting condensate of neutral fermions. This bending of the plasma branch to a linear dispersion when ω_p tends to 0 is similar to what happens in the normal phase, where the normal plasma branch tends to zero sound (with the difference that the velocity of zero sound is v_F instead of $v_F/\sqrt{3}$ here).

The most remarkable behavior occurs in between those two limits. First, the repulsion of the pair-breaking threshold leads to a squareroot divergence of $\text{Re } \alpha$ when approaching the pair-breaking threshold from below. This opens an interval $\omega_p \in [1.696\Delta, 2\Delta]$ where plasmons have an anomalous *negative* dispersion at the origin, that is, $\text{Re } \alpha < 0$. Then, at $\omega_p > 2\Delta$, Eq. (8) (with $\omega_p \rightarrow \omega_p + i0^+$) shows that α acquires an imaginary part that describes the nonzero damping rate of plasmons. This reflects the fact that a superconductor has pair-breaking decay channels available even at zero-temperature (unlike the particle-hole channels of the normal phase). Those channels are very active when ω_p is just above the pair-breaking threshold such that $\text{Im } \alpha$ shows a squareroot divergence when $\omega_p \rightarrow 2\Delta^+$. On the contrary, they weaken in the limit of large ω_p , such that $\text{Im } \alpha$ vanishes as $-16\pi \Delta^2 \epsilon_F / \omega_p^3$.

At nonzero temperature, plasmons are also sensitive to the quasiparticle-quasihole excitations. Equation (8) generalizes into

$$\alpha = \frac{\epsilon_F}{\Delta} \left[\frac{6\bar{\omega}_p}{5} (I_3 + J_0 - J_2) - \frac{8}{3\bar{\omega}_p} I_1 \right], \quad (10)$$

in terms of the dimensionless parameters $\bar{T} = T/\Delta$, $\bar{\omega}_p = \omega_p/\Delta$, and the integrals $I_n = \int_0^{+\infty} d\xi \frac{\text{th}(\epsilon/2\bar{T})}{\epsilon^n (\bar{\omega}_p^2 - 4\epsilon^2)}$ and $J_n = \frac{1}{2\bar{T}\bar{\omega}_p^2} \int_0^{+\infty} \frac{d\xi}{\epsilon^n \text{ch}^2(\epsilon/2\bar{T})}$ with $\epsilon = \sqrt{\xi^2 + 1}$. The red curve in Fig. 1 shows α in the vicinity of the critical temperature $T/T_c = 0.9989$ ($T/\Delta = 10$). We observe that α tends to its normal limit $6\epsilon_F/5\omega_p$ uniformly except in a neighborhood of size $\approx \Delta^2/T$ around 2Δ . There, the divergence of the real and imaginary parts is preserved whenever $T < T_c$, showing that a regime of anomalous plasmon dispersion subsists until the transition to the normal phase. In usual situations, ω_p is fixed in units of the Fermi energy ϵ_F , but the ratio $\omega_p/\Delta(T)$ can still be adjusted by varying the temperature. The negative plasma dispersion will thus eventually occur when increasing the temperature provided that ω_p is below 2Δ at $T = 0$.

One could be surprised that plasmons remain undamped ($\text{Im } \alpha = 0$) for $\omega_p < 2\Delta$ despite a nonzero temperature which provides a decay channel through quasiparticle-quasihole excitations. In fact, to absorb a plasmon (i.e., to satisfy the resonance condition $\omega_p = \epsilon_{\mathbf{q}+\mathbf{k}/2} - \epsilon_{\mathbf{q}-\mathbf{k}/2}$) quasiparticles need to have a wavenumber $k > 2m\omega_p/q$. The plasmon lifetime thus follows an activation law $\text{Im } z_q \propto e^{-2m\omega_p^2/q^2 T}$ which is exponentially suppressed in the limit $\Delta/\epsilon_F, T/\epsilon_F \rightarrow 0$ with ω_p, q of order $\Delta, 1/\xi$. Plasmon damping at $\omega_p < 2\Delta$ is thus essentially a strong-coupling effect.

IV. RESONANCE SPLITTING

Superconductivity not only bends the dispersion of the plasma branch, it also deforms the shape of the density response function $\chi_{33}(\omega)$ at frequencies close to the pair-breaking threshold. Besides the Lorentzian peak centered

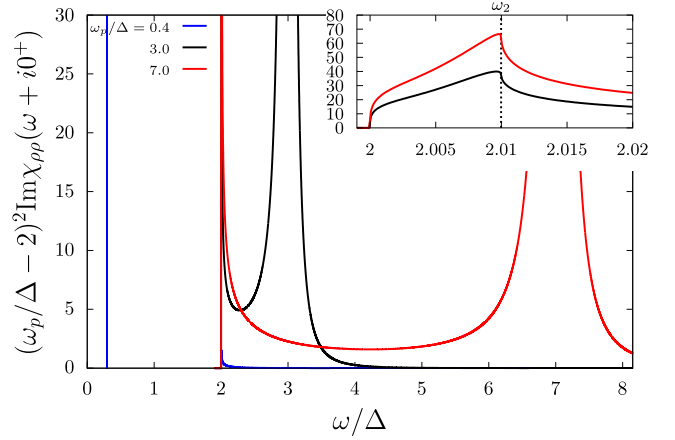


FIG. 2. Density-density response in function of the excitation frequency ω at fixed wave number $q\xi = 0.1$ and various plasma frequencies. For visibility, we have multiplied $\chi_{\rho\rho}$ by $(\omega_p/\Delta - 2)^2$. The inset is a zoom on the first peak in the interval $[2\Delta, \omega_2]$. On the blue curve, the Dirac peak is at $\omega \simeq 0.416\Delta$.

around $\text{Re } z_q \simeq \omega_p$, a second peak, shown on Fig. 2, emerges between 2Δ and the second branching point [15,23]

$$\omega_2 = \sqrt{4\Delta^2 + \epsilon_F \frac{q^2}{2m}}, \quad (11)$$

of the continuum. The peak is absent in the neutral case (which in our case corresponds to the limit $\omega_p \rightarrow 0$, see the blue curve in Fig. 2), and starts to grow as ω_p approaches 2Δ from below. It reaches its maximal intensity when ω_p passes 2Δ but the peak remarkably persists even in the regime $\omega_p \gg 2\Delta$ (although its spectral weight relative to the main plasma resonance decreases in this limit, red curve in Fig. 2). It thus seems as if a part of the spectral weight gets captured when ω_p passes the range $[2\Delta, \omega_2]$ and remains trapped in this range even when ω_p becomes large. Similarly to the disappearance of the phononic branch, this peak above 2Δ is thus a signature of long-range interactions, with the difference that it is specific to the superconducting state (whereas the Anderson mechanism occurs also in the normal phase).

The behavior of this peak becomes clearer when looking at the analytic structure of χ_{33} . The Riemann sheet connected to the interval $[2\Delta, \omega_2]$ of the real axis contains a unique pole of the density-phase propagator at

$$z_q^{\text{II}} = 2\Delta - \frac{i + \text{sign}(2\Delta - \omega_p)}{\sqrt{\Delta}} \sqrt{\frac{8}{3\pi^2} \left| 1 - \frac{4\Delta^2}{\omega_p^2} \right|} \left(\frac{k_F q}{2m} \right)^{3/2} + O(q^{7/4}). \quad (12)$$

This pole should not be confused with the famous amplitude ‘‘Higgs’’ mode [2,23,26]; although both poles lie in the same energy range $[2\Delta, \omega_2]$, they concern excitation channels (the density-phase channel for z_q^{II} , the modulus channel for the amplitude mode) which are decoupled in the weak-coupling limit. Equation (12) exhibits an unusual noninteger power-law

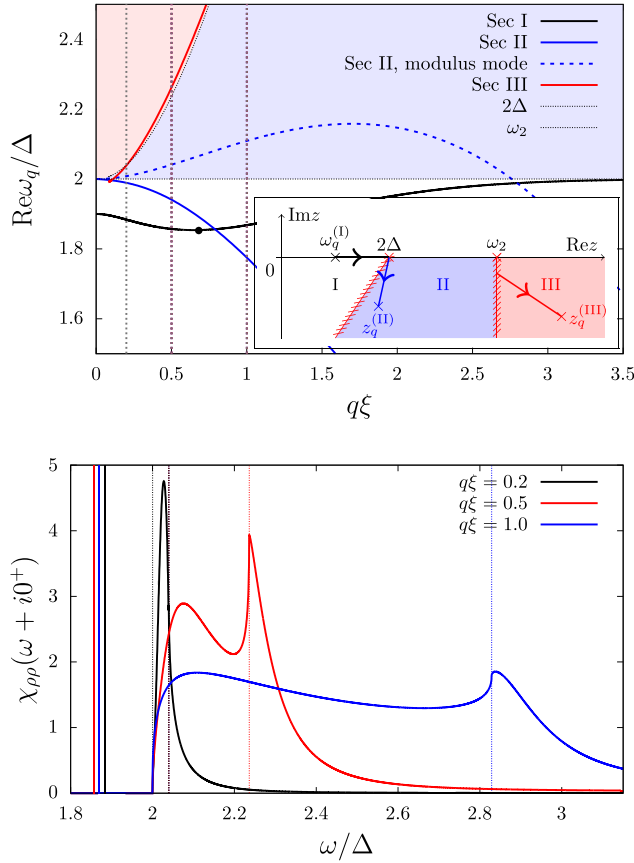


FIG. 3. (Top panel) Eigenfrequency $\text{Re}z_q$ of the plasma branch in function of the wave vector q (in unit of the inverse pair radius $\xi = k_F/2m\Delta$), with $\omega_p = 1.9\Delta$. The angular points 2Δ and ω_2 [Eq. (11)] are shown as dotted lines. The analytic windows are shown in colors: white for $\omega < \omega_1$ (window I), blue for $\omega_1 < \omega < \omega_2$ (window II) and red for $\omega > \omega_2$ (window III). The solution of Eq. (5) in each window is shown as a solid line in the corresponding color. The inset shows their schematic trajectories in the complex plane after analytic continuation. In window II, the pair-breaking mode (solution of $M_{22,\downarrow} = 0$) is shown as a dashed line. The dispersion minimum of the undamped solution below 2Δ is shown by the black dot. (Bottom panel) Density-density response in function of the excitation frequency ω at fixed plasma frequency $\omega_p = 1.9\Delta$ and excitation wave number $q = 0.2/\xi$, 0.5ξ , and 1.0ξ (corresponding to the vertical dotted lines in the top panel). The angular points 2Δ and $\omega_2(q)$ are marked by vertical dotted lines. Besides the Dirac peaks below 2Δ , broadened peaks are visible inside the pair-breaking continuum.

dispersion², which contrasts with the quadratic dispersion of the plasma and amplitude modes.

The real part of z_q^{II} is either below 2Δ when $\omega_p < 2\Delta$ or above ω_2 when $\omega_p > 2\Delta$. This explains why the associated peak fades at low ω_p (and disappears in the neutral case), and

²When $\omega_p = 2\Delta$ the quadratic law reemerges $z_q^{\text{II}} = 2\Delta - (0.0184 + 0.9953i)\frac{\epsilon_F}{\Delta}\frac{q^2}{2m} + O(q^4)$. This result, like Eq. (12), is obtained by expanding at low q as prescribed by Eq. (10) in Ref. [23].

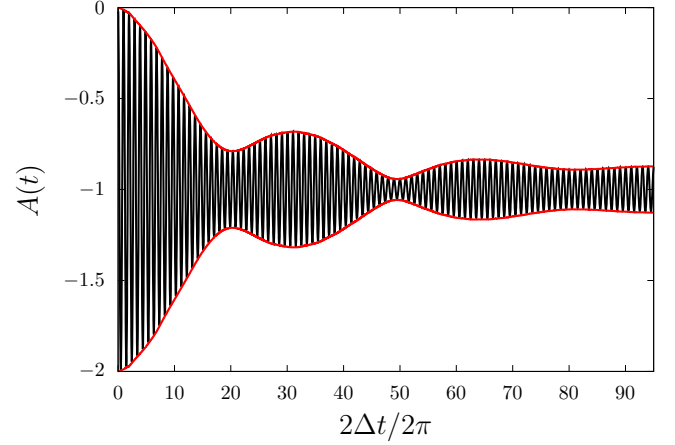


FIG. 4. Time-evolution of the amplitude $A(t) = 2V_C(q)\delta\rho(\mathbf{r}, t)/u_0 \cos(\mathbf{q} \cdot \mathbf{r})$ of a density wave created by a sudden excitation. We have used here $q\xi = 0.1$ and $\omega_p = 2.05\Delta$.

has its maximum in ω_2 for $\omega_p > 2\Delta$, as shown by the inset of Fig. 2. Equation (12) behaves well in the limit $\omega_p/\Delta \rightarrow +\infty$, which confirms that the peak near the continuum edge survives in this limit.

Figure 3 summarizes the analytic structure of χ_{33} . The function is divided in three analyticity windows (I, II, and III) by its two branching points 2Δ and ω_2 . Each window is associated to a separate Riemann sheet (inset of Fig. 3) each containing a single pole of the density-phase propagator (respectively ω_q^{I} , z_q^{II} , and z_q^{III}). Conversely, χ_{22} only has a pole in sheet II, corresponding to the amplitude mode (dashed blue line). Here, for $\omega_p = 1.9\Delta$, the real pole ω_q^{I} supports the main plasma branch departing in ω_p (while for $\omega_p > 2\Delta$ the main branch would be supported by z_q^{III}), z_q^{II} is below 2Δ , and z_q^{III} follows rather closely the angular point ω_2 .

V. BEATING OF DENSITY WAVES

In the frequency domain, we have described an unusual splitting of the plasma resonance into a peak around ω_p and a peak in the range $[2\Delta, \omega_2]$. To further illustrate the originality of this phenomenon, we study its counter-part in the time-domain, through the relaxation of abrupt density perturbations. Namely, we suppose that at $t > 0$ an operator suddenly turns on a static external field $u_\rho(\mathbf{r}) = u_0 \cos(\mathbf{q} \cdot \mathbf{r})$ coupled to the electronic density. The subsequent evolution of the density perturbation is given by the inverse Laplace transform of the density-density response function:

$$\delta\rho(\mathbf{r}, t) = \frac{u_0 \cos(\mathbf{q} \cdot \mathbf{r})}{2V_C(q)} \int_{+\infty+i\eta}^{-\infty-i\eta} \frac{dz}{2i\pi} \frac{e^{-izt}}{z} \chi_{33}(z, \mathbf{q}). \quad (13)$$

This integral can be closed into a winding contour around the branch cut $[2\Delta, +\infty[$ and a residue in the real pole ω_q^{I} . The time-evolution of $\delta\rho$ thus combines the contributions of the plasmonic resonance and of the peak near the continuum edge, which causes the system to oscillate at multiple frequencies. As shown on Fig. 4, when the two peaks are close (we use here $\omega_p = 2.05\Delta$) this leads to very remarkable beatings, with a carrier oscillating at frequency $\omega_p \approx 2\Delta$ modulated by an

envelope of typical frequency $|\omega_p - 2\Delta| \ll 2\Delta$. As the contribution of the pair-breaking continuum to Eq. (13) decays with time, the beatings gradually disappear and give way to undamped oscillations at frequency ω_q^l (very close to 2Δ here) about the static response $\delta\rho(\mathbf{r}, t) = -\frac{u_0 \cos(\mathbf{q}\cdot\mathbf{r})}{2v_c(q)}$.

VI. CONCLUSION

We have described the low- q dispersion of superconducting plasmons in 3D, revealing a regime of anomalous downward dispersion, and a finite lifetime due to the pair-breaking decay channels. A new resonance also emerges near the pair-breaking threshold, indicating a splitting of density waves into high- and low-frequency components. For a more realistic description of plasmons in cuprates, our study should be extended to 2D superconductors [28], or 2D-layered electron gases [14,17,29]. Our work may also be applied to

superfluids of ultracold fermions [30] where different kinds of long-range interactions can be engineered [31], or neutron star matter [10].

ACKNOWLEDGMENTS

We acknowledge financial support from the Research Foundation-Flanders (FWO-Vlaanderen) Grant No. G.0618.20.N, and from the research council of the University of Antwerp.

APPENDIX A: BARE PROPAGATOR

Here, we recall the expression of the bare propagator Π which is used to construct the response function χ . The matrix elements can be expressed in a generic form

$$\Pi_{ij}(z, \mathbf{q}) = \sum_{\mathbf{k}} \frac{1}{2\epsilon_+\epsilon_-} \left[\frac{(1-f_+ - f_-)\pi_{ij}^+}{z^2 - (\epsilon_+ + \epsilon_-)^2} - \frac{(f_+ - f_-)\pi_{ij}^-}{z^2 - (\epsilon_+ - \epsilon_-)^2} \right], \quad (\text{A1})$$

with $\xi_{\pm} = (\mathbf{q}/2 \pm \mathbf{k})^2/2m - \mu$, $\epsilon_{\pm} = \sqrt{\xi_{\pm}^2 + \Delta^2}$ and $f_{\pm} = 1/(1 + e^{\epsilon_{\pm}/T})$, and the (symmetric) matrices of coefficients

$$\pi^+ = \begin{pmatrix} (\epsilon_+ + \epsilon_-)(\epsilon_+\epsilon_- + \xi_+\xi_- + \Delta^2) & z(\epsilon_-\xi_+ + \epsilon_+\xi_-) & -z(\epsilon_+ + \epsilon_-) \\ * & (\epsilon_+ + \epsilon_-)(\epsilon_+\epsilon_- + \xi_+\xi_- - \Delta^2) & -(\epsilon_+ + \epsilon_-)(\xi_+ + \xi_-) \\ * & * & (\epsilon_+ + \epsilon_-)(\epsilon_+\epsilon_- - \xi_+\xi_- + \Delta^2) \end{pmatrix}, \quad (\text{A2})$$

$$\pi^- = \begin{pmatrix} (\epsilon_+ - \epsilon_-)(\epsilon_+\epsilon_- - \xi_+\xi_- - \Delta^2) & z(\epsilon_-\xi_+ - \epsilon_+\xi_-) & z(\epsilon_+ - \epsilon_-) \\ * & (\epsilon_+ - \epsilon_-)(\epsilon_+\epsilon_- - \xi_+\xi_- + \Delta^2) & (\epsilon_+ - \epsilon_-)(\xi_+ + \xi_-) \\ * & * & (\epsilon_+ - \epsilon_-)(\epsilon_+\epsilon_- + \xi_+\xi_- - \Delta^2) \end{pmatrix}. \quad (\text{A3})$$

To compute the matrix $M = \Pi - D$ in long-wave limit, we perform a combination of lines and columns:

$$N = \begin{pmatrix} M_{11} & M_{12} & zM_{13} + 2M_{11} \\ M_{12} & M_{22} & zM_{23}/\Delta + 2M_{12} \\ zM_{13}/\Delta + 2M_{11} & zM_{23}/\Delta + 2M_{12} & z^2M_{33}/\Delta^2 + 4zM_{13}/\Delta + 4M_{11} \end{pmatrix}. \quad (\text{A4})$$

The advantage of this recombined matrix is that the whole third line and column is of order q^2 . Explicitly,

$$N_{13} = \sum_{\mathbf{k}} \frac{2\xi_+\xi_- - \xi_+^2 - \xi_-^2}{2\epsilon_+\epsilon_-} \left[\frac{(1-f_+ - f_-)(\epsilon_+ + \epsilon_-)}{z^2 - (\epsilon_+ + \epsilon_-)^2} + \frac{(f_+ - f_-)(\epsilon_+ - \epsilon_-)}{z^2 - (\epsilon_+ - \epsilon_-)^2} \right], \quad (\text{A5})$$

$$N_{23} = -\sum_{\mathbf{k}} \frac{z(\xi_+ - \xi_-)}{2\epsilon_+\epsilon_-} \left[\frac{(1-f_+ - f_-)(\epsilon_+ - \epsilon_-)}{z^2 - (\epsilon_+ + \epsilon_-)^2} + \frac{(f_+ - f_-)(\epsilon_+ + \epsilon_-)}{z^2 - (\epsilon_+ - \epsilon_-)^2} \right], \quad (\text{A6})$$

$$\begin{aligned} \Delta^2 N_{33} &= \frac{\rho L^3 q^2}{2m} \left(1 - \frac{z^2}{\omega_p^2} \right) + \sum_{\mathbf{k}} \frac{(\xi_+ - \xi_-)^2}{2\epsilon_+\epsilon_-} \left[\frac{(\epsilon_+ + \epsilon_-)(1-f_+ - f_-)(\epsilon_+\epsilon_- - \xi_+\xi_- - \Delta^2)}{z^2 - (\epsilon_+ + \epsilon_-)^2} \right. \\ &\quad \left. - \frac{(\epsilon_+ - \epsilon_-)(f_+ - f_-)(\epsilon_+\epsilon_- + \xi_+\xi_- + \Delta^2)}{z^2 - (\epsilon_+ - \epsilon_-)^2} \right]. \end{aligned} \quad (\text{A7})$$

Note that the expression of N_{33} has been simplified using the sum rule found in Ref. [9], namely

$$\sum_{\mathbf{k}} \frac{(1-f_+ - f_-)(\epsilon_+ + \epsilon_-)(\epsilon_+\epsilon_- - \xi_+\xi_- - \Delta^2) - (f_+ - f_-)(\epsilon_+ - \epsilon_-)(\epsilon_+\epsilon_- + \xi_+\xi_- + \Delta^2)}{2\epsilon_+\epsilon_-} = \frac{\rho V q^2}{2m}. \quad (\text{A8})$$

Thus, to leading order in q , the eigenenergy of the plasma branch solves $N_{33}(z_q, q) = 0$, which yields immediately Eq. (7) of the main text.

APPENDIX B: LOW- q EXPANSION OF THE FLUCTUATION MATRIX

We give additional detail on the low- q expansion of M , which leads to Eqs. (8) and (10) of the dispersion parameter

TABLE I. Long-wavelength expansion of the elements of N in terms of the function g of Eq. (B3) (at $T = 0$) and of the integrals I_n and J_n defined below Eq. (10) (at $T \neq 0$).

Coefficient	At $T = 0$	At $T \neq 0$
$n_{33}^{(0)}$	0	0
$n_{33}^{(2)}$	$\frac{2}{3}(1 - \frac{\bar{z}^2}{\bar{\omega}_p^2})$	$\frac{2}{3}(1 - \frac{\bar{z}^2}{\bar{\omega}_p^2})$
$n_{33}^{(4)}$	$\frac{8(4g+1)}{5\bar{z}^2}$	$\frac{8}{5}(I_3 - J_2 + J_0)$
$n_{33}^{(6)}$	$\frac{32(-8\bar{z}g' + 8(\bar{z}^2 - 1)g + \bar{z}^2 - 2)}{7\bar{z}^6}$	
$n_{11}^{(0)}$	$\frac{\bar{z}^2 g}{2}$	$\frac{\bar{z}^2 I_1}{2}$
$n_{11}^{(2)}$	$-\frac{4\bar{z}g' + 4g + 1}{3\bar{z}^2}$	
$n_{13}^{(0)}$	0	0
$n_{13}^{(2)}$	$-\frac{4g}{3}$	$-\frac{4}{3}I_1$
$n_{13}^{(4)}$	$\frac{8(4\bar{z}g' - 2(\bar{z}^2 - 2)g + 1)}{5\bar{z}^4}$	

in the main text. In this Appendix, we use the dimensionless variables $\bar{q} = q\xi$, $\bar{z} = z/\Delta$ and

$$n_{ij} = N_{ij} \times (2\pi)^3 \epsilon_F / k_F^3 L^3. \quad (\text{B1})$$

Generically, the expansion of a matrix element can be written as

$$n_{ij} = \sum_{p=0}^n n_{ij}^{(p)}(\bar{z}) q^{2p} + O(q^{2(n+1)}), \quad (\text{B2})$$

and all coefficients $n_{ij}^{(p)}$ are elementary functions of \bar{z} , of the function

$$g(\bar{z}) = \begin{cases} -\frac{\arcsin(\bar{z}/2)}{\bar{z}\sqrt{4-\bar{z}^2}} & \text{if } \bar{z} < 2 \\ \frac{\operatorname{argcosh}(\bar{z}/2)}{\bar{z}\sqrt{\bar{z}^2-4}} - \frac{i\pi}{2\bar{z}\sqrt{\bar{z}^2-4}} & \text{if } \bar{z} > 2, \end{cases} \quad (\text{B3})$$

and its derivative. Their explicit expression is given in Table I.

At $T = 0$, we have derived the coefficient of the term in q^4 in the plasma dispersion (such that $z_q = \omega_0 + \alpha \frac{q^2}{2m} + \frac{\beta}{\epsilon_F} (\frac{q^2}{2m})^2 + O(q^6)$):

$$\beta = \frac{\epsilon_F^3}{\omega_p^3} h\left(\frac{\omega_p}{\Delta}\right), \quad (\text{B4})$$

with

$$h(\omega) = \frac{1}{1575\omega^2} [64\omega g'(\omega)(112\omega^2 g(\omega) + 63\omega^2 - 220) - 10(32g(\omega)(56\omega^2 g(\omega) - 9\omega^2 + 44) + 27\omega^2 + 352)]. \quad (\text{B5})$$

This coefficient β is positive in the interval $[1.696\Delta, 2\Delta]$ where α is negative, which allows us to estimate the position of the dispersion minimum as

$$q_{\min} \xi \approx \sqrt{-\frac{\epsilon_F^2}{\Delta^2} \frac{\alpha}{2\beta}}. \quad (\text{B6})$$

Figure 5 show the dependence of q_{\min} on the ratio ω_p/Δ , using both (B6) and the exact numerical solution.

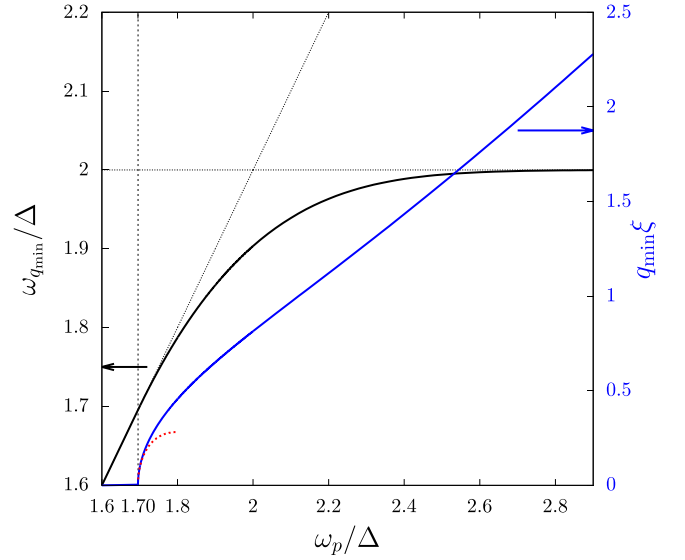


FIG. 5. The dispersion minimum $\omega_{q_{\min}}$ and the wavenumber q_{\min} at which it is reached in function of the plasma frequency. For $\omega_p < 1.696$, q_{\min} is identically 0 and $\omega_{q_{\min}}$ coincides with ω_p (oblique dotted line). Then for $\omega_p > 1.696$, q_{\min} departs from 0 as described by Eq. (B6) (dashed red curve). In the limit $\omega_p \rightarrow +\infty$, q_{\min} diverges linearly and $\omega_{q_{\min}}$ tends to 2Δ .

APPENDIX C: NUMERICAL IMPLEMENTATION

Here we give additional details on how to evaluate the matrix M numerically at $T = 0$ but arbitrary values of $q\xi$. The associated Fortran code is available online [32]. The rigorous way to take the BCS limit ($\Delta \rightarrow 0$) and to deal with the resonance condition is explained in Ref. [24]. For $\Delta \rightarrow 0$ and fixed $\bar{q} = q\xi$, $\bar{\omega} = \omega/\Delta$, the momentum integrals defining the matrix element M_{ij} are dominated by wavevectors close to the dispersion minimum $k_0 = \sqrt{2m\mu} \simeq k_F$. We thus set $\bar{\xi} = \xi_k/\Delta$, $kdk/2m\Delta = d\bar{\xi}/2$, and expand the integrand for $k_0 \gg \sqrt{2m\Delta}$.

The integral over $\bar{\xi}$ from $-\infty$ to $+\infty$ is odd in the case of M_{12} and M_{23} (which therefore vanish), and even otherwise. The spectral density associated to m_{ij} [the dimensionless version of M_{ij} , see Eq. (B1)] takes the form

$$\rho_{ij}(\bar{\omega}) = \int_0^{+\infty} d\bar{\xi} \int_0^1 du \bar{\pi}_{ij}^+ \delta(\bar{\omega} - \bar{\epsilon}_+ - \bar{\epsilon}_-), \quad (\text{C1})$$

with

$$\bar{\pi}_{11}^+ = \bar{\epsilon}_+ \bar{\epsilon}_- + \bar{\xi}_+ \bar{\xi}_- + 1, \quad (\text{C2})$$

$$\bar{\pi}_{22}^+ = \bar{\epsilon}_+ \bar{\epsilon}_- + \bar{\xi}_+ \bar{\xi}_- - 1, \quad (\text{C3})$$

$$\bar{\pi}_{33}^+ = \bar{\epsilon}_+ \bar{\epsilon}_- - \bar{\xi}_+ \bar{\xi}_- + 1, \quad (\text{C4})$$

$$\bar{\pi}_{13}^+ = -\bar{\epsilon}_+ - \bar{\epsilon}_-. \quad (\text{C5})$$

We use here (and everywhere in this Appendix) the dimensionless notations $\bar{\xi}_{\pm} = \xi_{q/2 \pm k}/\Delta = \bar{\xi} \pm u\bar{q}$ and $\bar{\epsilon}_{\pm} = \sqrt{\bar{\xi}_{\pm}^2 + 1}$.

We use the Dirac delta to integrate over $\bar{\xi}$ at fixed u . The resonance condition ($\omega = \epsilon_+ + \epsilon_-$) is studied in Annexe A. of Ref. [24]. On the interval $[0, +\infty[$, it yields a unique root:

$$\bar{\xi}_0 = \frac{\bar{\omega}}{2} \frac{r_2}{r_1} \text{ with } r_1 = \sqrt{\bar{\omega}^2 - 4\bar{q}^2 u^2}$$

and $r_2 = \sqrt{\bar{\omega}^2 - 4\bar{q}^2 u^2 - 4}$, (C6)

$\bar{\xi}_0$ is real provided

$$u < u_{\max} = \left(\frac{\bar{\omega}^2 - 4}{4\bar{q}^2} \right)^{1/2}, \quad (C7)$$

such that the remaining interval of integration over u is

$$I_u(\omega) = \begin{cases} \emptyset & \text{if } \bar{\omega} < 2 \\ [0, u_{\max}] & \text{if } 2 < \bar{\omega} < \bar{\omega}_2 \\ [0, 1] & \text{if } \bar{\omega} > \bar{\omega}_2 \end{cases} \quad (C8)$$

where $\bar{\omega}_2 = 2\sqrt{1 + \bar{q}^2}$ is the dimensionless version of Eq. (11). After integration over ξ , we obtain

$$\rho_{ij} = \int_{I_u(\omega)} r_{ij}(u) du, \quad (C9)$$

with the integrands r_{ij} :

$$r_{11} = \frac{r_1}{4r_2} \quad (C10)$$

$$r_{22} = \frac{r_2}{4r_1} \quad (C11)$$

$$r_{33} = \frac{\bar{\omega}^2}{r_1^3 r_2} \quad (C12)$$

$$r_{13} = \frac{\bar{\omega}}{2r_1 r_2} \quad (C13)$$

The angular integrals (C9) can be computed analytically in terms of elliptic integrals (denoted in the convention of Ref. [33]). For $2 < \bar{\omega} < \bar{\omega}_2$, we set $m = \sqrt{\bar{\omega}^2 - 4}/\bar{\omega}$, and obtain:

$$\rho_{11} = \rho_{33} = \frac{\bar{\omega}}{8\bar{q}} E(m) \quad (C14)$$

$$\rho_{13} = \frac{K(m)}{4\bar{q}} \quad (C15)$$

$$\rho_{22} = \rho_{11} - \frac{2}{\bar{\omega}} \rho_{13} \quad (C16)$$

For $\bar{\omega} > \bar{\omega}_2$, we perform the change of variable $\sin \phi = \sqrt{\bar{\omega}^2 - 4u}/2\bar{q}$. Introducing $\theta = \arcsin(2\bar{q}/\sqrt{\bar{\omega}^2 - 4})$, we have

$$\rho_{11} = \frac{\bar{\omega}}{8\bar{q}} E(\theta, m) \quad (C17)$$

$$\rho_{13} = \frac{F(\theta, m)}{4\bar{q}} \quad (C18)$$

$$\rho_{22} = \rho_{11} - \frac{2}{\bar{\omega}} \rho_{13} \quad (C19)$$

$$\rho_{33} = \rho_{11} - \sqrt{\frac{\bar{\omega}^2 - 4\bar{q}^2 - 4}{\bar{\omega}^2 - 4\bar{q}^2}} \quad (C20)$$

Once the spectral densities are known, the value of m at arbitrary z is given by frequency integrals

$$m_{ii}(\bar{z}) = \int_2^{+\infty} d\bar{\omega} \left(\rho_{ii}(\bar{\omega}) \left[\frac{1}{\bar{z} - \bar{\omega}} - \frac{1}{\bar{z} + \bar{\omega}} \right] + \frac{1}{2\sqrt{\bar{\omega}^2 - 4}} \right)$$

for $i = 1, 2$ (C21)

$$m_{33}(\bar{z}) = \int_2^{+\infty} d\bar{\omega} \left[\rho_{33}(\bar{\omega}) \left[\frac{1}{\bar{z} - \bar{\omega}} - \frac{1}{\bar{z} + \bar{\omega}} \right] \right] - \frac{2\bar{q}^2}{3\bar{\omega}_p^2} \quad (C22)$$

$$m_{13}(\bar{z}) = \int_2^{+\infty} d\bar{\omega} \left[\rho_{13}(\bar{\omega}) \left[\frac{1}{\bar{z} - \bar{\omega}} + \frac{1}{\bar{z} + \bar{\omega}} \right] \right] \quad (C23)$$

where we have used the trick of Ref. [24] to handle the regularizing counter-term $-V/g$: we subtract $M_{11}(\omega = 0, \mathbf{q}) = 0$ to $M_{11}(\omega, \mathbf{q})$ and $M_{22}(\omega = 2\Delta, \mathbf{q}) = 0$ to $M_{22}(\omega, \mathbf{q})$ and we use the expression of the spectral densities at zero wave vector $\rho_{22}(\bar{\omega}, 0) = \sqrt{\bar{\omega}^2 - 4}/4\bar{\omega}$ and $\rho_{11}(\bar{\omega}, 0) = \bar{\omega}/4\sqrt{\bar{\omega}^2 - 4}$. We have used also the (im)parity of the spectral densities $\rho_{ii}(-\bar{\omega}) = \rho_{ii}(\bar{\omega})$ and $\rho_{13}(-\bar{\omega}) = -\rho_{13}(\bar{\omega})$.

Note that the integral forms [Eqs. (C21)–(C23)] remain valid in the vicinity of the real axis ($\bar{z} = \bar{\omega}_0 + i0^+$), in which case they should be understood as principal parts. To deal with the cancellation of the denominator, we write

$$\mathcal{P} \int_{\omega_1}^{\omega_2} d\omega \frac{\rho_{ij}(\omega)}{\omega_0 - \omega} = \int_{\omega_1}^{\omega_2} d\omega \frac{\rho_{ij}(\omega) - \rho_{ij}(\omega_0)}{\omega_0 - \omega} - \rho_{ij}(\omega_0) \log \left| \frac{\omega_0 - \omega_2}{\omega_0 - \omega_1} \right|. \quad (C24)$$

To reach a good precision on the integrand, one should be careful to split it at its angular point $\bar{\omega}_2$. A change of variable may also be needed to handle the $1/\sqrt{\bar{\omega} - 2}$ divergence at the continuum edge.

Analytic continuation. To analytically continue M through window II or III, we use the formula of Nozières:

$$m_{\downarrow}^{(\text{II or III})}(z, \mathbf{q}) = \begin{cases} m(\bar{z}, \bar{q}), & \text{Im } z > 0 \\ m(\bar{z}, \bar{q}) - 2i\pi \rho_{\downarrow}^{(\text{II or III})}(\bar{z}, \bar{q}), & \text{Im } z < 0, \end{cases} \quad (C25)$$

where $\rho_{\downarrow}^{(\text{II or III})}$ is the analytic continuation of the spectral density from the interval $[2, \bar{\omega}_2]$ or $[\bar{\omega}_2, +\infty[$ onto the lower-half complex plane. In practice, it is much easier to analytically continue ρ than M directly, which is why the formula of Nozières is useful. In the present case, it is enough to complexify the integral expression [Eq. (C9)]. This means that (i) the integrand becomes complex (in particular because the resonance energy $\bar{\xi}_0$ becomes complex), and (ii) the integration interval I_u can become a contour in the complex plane. This contour can be deformed to optimize the convergence of the integral (as long as one stays away from the branching points of the integrand).

- [1] M.-A. Méasson, Y. Gallais, M. Cazayous, B. Clair, P. Rodière, L. Cario, and A. Sacuto, *Phys. Rev. B* **89**, 060503(R) (2014).
- [2] R. Grasset, Y. Gallais, A. Sacuto, M. Cazayous, S. Mañas-Valero, E. Coronado, and M.-A. Méasson, *Phys. Rev. Lett.* **122**, 127001 (2019).
- [3] R. Matsunaga, Y. I. Hamada, K. Makise, Y. Uzawa, H. Terai, Z. Wang, and R. Shimano, *Phys. Rev. Lett.* **111**, 057002 (2013).
- [4] P. W. Anderson, *Phys. Rev.* **112**, 1900 (1958).
- [5] H. A. Fertig and S. Das Sarma, *Phys. Rev. B* **44**, 4480 (1991).
- [6] R. Côté and A. Griffin, *Phys. Rev. B* **48**, 10404 (1993).
- [7] S. Artemenko and A. Kobel'kov, *Physica C: Superconductivity* **253**, 373 (1995).
- [8] D. van der Marel, *Phys. Rev. B* **51**, 1147 (1995).
- [9] Y. Ohashi and S. Takada, *J. Phys. Soc. Jpn.* **67**, 551 (1998).
- [10] M. Baldo and C. Ducoin, *Phys. At. Nucl.* **74**, 1508 (2011).
- [11] K. Tamasaku, Y. Nakamura, and S. Uchida, *Phys. Rev. Lett.* **69**, 1455 (1992).
- [12] O. Buisson, P. Xavier, and J. Richard, *Phys. Rev. Lett.* **73**, 3153 (1994).
- [13] K. Kadowaki, I. Kakeya, M. B. Gaifullin, T. Mochiku, S. Takahashi, T. Koyama, and M. Tachiki, *Phys. Rev. B* **56**, 5617 (1997).
- [14] A. Nag, M. Zhu, M. Bejas, J. Li, H. C. Robarts, H. Yamase, A. N. Petsch, D. Song, H. Eisaki, A. C. Walters *et al.*, *Phys. Rev. Lett.* **125**, 257002 (2020).
- [15] E. H. Hwang and S. Das Sarma, *Phys. Rev. B* **52**, R7010 (1995).
- [16] F. J. Dunmore, D. Z. Liu, H. D. Drew, S. Das Sarma, Q. Li, and D. B. Fenner, *Phys. Rev. B* **52**, R731 (1995).
- [17] H. Shibata and T. Yamada, *Phys. Rev. Lett.* **81**, 3519 (1998).
- [18] A. Dienst, E. Casandruc, D. Fausti, L. Zhang, M. Eckstein, M. Hoffmann, V. Khanna, N. Dean, M. Gensch, S. Winnerl *et al.*, *Nat. Mater.* **12**, 535 (2013).
- [19] H. T. Stinson, J. S. Wu, B. Y. Jiang, Z. Fei, A. S. Rodin, B. C. Chapler, A. S. McLeod, A. Castro Neto, Y. S. Lee, M. M. Fogler *et al.*, *Phys. Rev. B* **90**, 014502 (2014).
- [20] E. A. Pashitskii and V. I. Pentegov, *Low Temp. Phys.* **34**, 113 (2008).
- [21] M. M. Doria, G. Hollauer, F. Parage, and O. Buisson, *Phys. Rev. B* **56**, 2722 (1997).
- [22] H. Kurkjian, J. Tempere, and S. N. Klimin, *Sci. Rep.* **10**, 11591 (2020).
- [23] H. Kurkjian, S. N. Klimin, J. Tempere, and Y. Castin, *Phys. Rev. Lett.* **122**, 093403 (2019).
- [24] Y. Castin and H. Kurkjian, *Comptes Rendus. Physique* **21**, 253 (2020).
- [25] S. N. Klimin, J. Tempere, and H. Kurkjian, *Phys. Rev. A* **100**, 063634 (2019).
- [26] V. A. Andrianov and V. N. Popov, *Teor. Matemat. Fiz.* **28**, 341 (1976) [*Theor. Math. Phys.* **28**, 829 (1976)].
- [27] A. L. Fetter and J. D. Walecka, *Quantum theory of many-particle systems* (McGraw-Hill, San Francisco, 1971).
- [28] Z. Sun, M. M. Fogler, D. N. Basov, and A. J. Millis, *Phys. Rev. Res.* **2**, 023413 (2020).
- [29] R. Guo, S. Duan, Z. He, X. Liang, Z. Niu, M. He, Y. Jiang, J. Wu, L. Ji, B. Jin *et al.*, *Adv. Funct. Mater.* **31**, 2106891 (2021).
- [30] W. Zwerger (Ed.), *The BCS-BEC Crossover and the Unitary Fermi Gas* (Springer, Berlin, 2012).
- [31] L. Chomaz, R. M. W. van Bijnen, D. Petter, G. Faraoni, S. Baier, J. H. Becher, M. J. Mark, F. Wächtler, L. Santos, and F. Ferlaino, *Nat. Phys.* **14**, 442 (2018).
- [32] Github repository codearxiv_2201_11421, https://github.com/hkurkjian/codeArxiv_2201_11421, accessed: July 1st, 2022.
- [33] I. S. Gradshteyn and I. M. Ryzhik, *Tables of Integrals, Series, and Products* (Academic Press, San Diego, 1994).